



## Bone-targeted pH-responsive cerium nanoparticles for anabolic therapy in osteoporosis

Ce Dou<sup>a,b</sup>, Jianmei Li<sup>b</sup>, Jian He<sup>b</sup>, Fei Luo<sup>a</sup>, Tao Yu<sup>a</sup>, Qijie Dai<sup>a</sup>, Yueqi Chen<sup>a</sup>, Jianzhong Xu<sup>a,\*\*</sup>, Xiaochao Yang<sup>b,\*\*\*</sup>, Shiwu Dong<sup>b,c,\*</sup>

<sup>a</sup> Department of Orthopedics, Southwest Hospital, Third Military Medical University (Army Medical University), Chongqing, 400038, China

<sup>b</sup> Department of Biomedical Materials Science, Third Military Medical University (Army Medical University), Chongqing, 400038, China

<sup>c</sup> State Key Laboratory of Trauma, Burns and Combined Injury, Third Military Medical University (Army Medical University), Chongqing, 400038, China

### ARTICLE INFO

#### Keywords:

pH-responsive  
Nanomedicine  
Bone  
Osteoclast  
Anabolic therapy

### ABSTRACT

Antiresorptive drugs are widely used for treatment of osteoporosis and cancer bone metastasis, which function mainly through an overall inhibition of osteoclast. However, not all osteoclasts are “bone eaters”; preosteoclasts (pOCs) play anabolic roles in bone formation and angiogenesis through coupling with osteoblasts and secreting platelet derived growth factor-BB (PDGF-BB). In this study, a bone-targeted pH-responsive nanomaterial was designed for selectively eliminating mature osteoclasts (mOCs) without affecting pOCs. Biocompatible cerium nano-system (CNS) was guided to the acidic extracellular microenvironment created by mOCs and gained oxidative enzymatic activity. Oxidative CNS decreased the viability of mOCs through accumulating intracellular reactive oxygen species and enhancing calcium oscillation. Non-acid secreting anabolic pOCs were thus preserved and kept producing PDGF-BB, which lead to mesenchymal stem cell osteogenesis and endothelial progenitor cell angiogenesis via PI3K-Akt activated focal adhesion kinase. In treating osteoporotic ovariectomized mice, CNS showed better protective effects compare with the current first line antiresorptive drug due to the better anabolic effects marked by higher level of bone formation and vascularization. We provided a novel anabolic therapeutic strategy in treating bone disorders with excessive bone resorption.

### 1. Introduction

Mature osteoclasts are bone-specific polykaryons derived from multipotent hematopoietic stem cells and differentiated from monocyte/macrophage precursor cells near the bone surface [1]. Two important regulating factors, receptor activator of nuclear factor  $\kappa$ B ligand (RANKL) and macrophage-colony stimulating factor (M-CSF) are necessary for OC differentiation and survival [2,3]. Binding of RANKL to its ligand results in the initiation of the TNF receptor-associated factor (TRAF) 6 signaling, which eventually activates nuclear factor of activated T cells c1 (NFATc1), the master regulator in osteoclastogenesis [4, 5], leading to OC differentiation and maturation [6,7]. In human body, OC has a relatively short cell life of about 2 weeks. In this period, OC differentiates from mononuclear preosteoclast (pOC) to multinuclear

mature OC (mOC) and eventually undergoes apoptosis [8]. Dysregulation of osteoclastogenesis leads to various bone disorders such as tumor bone metastasis and osteoporosis [9–11].

The International Osteoporosis Foundation reported that more than 200 million people suffer from osteoporosis worldwide [12,13]. According to the review study of American Society for Bone and Mineral Research (ASBMR), long-term use (over 5 years) of bisphosphonates (BPs), the most commonly used medications for osteoporosis, can lead to unsatisfactory clinical outcomes and complications including atypical fractures and decrease of bone strength [14]. The detailed reasons for this side effect of BPs are still unclear, but we recently reported that alendronate, a nitrogen-containing bisphosphonate, triggers cell death in pOC through peroxisome dysfunction and further endoplasmic reticulum (ER) stress [15]. However, according to recent discoveries, pOC

Peer review under responsibility of KeAi Communications Co., Ltd.

\* Corresponding author. Department of Biomedical Materials Science, School of Biomedical Engineering, Third Military Medical University (Army Medical University), Chongqing, 400038, China.

\*\* Corresponding author.

\*\*\* Corresponding author.

E-mail addresses: [xujianzhong1962@163.com](mailto:xujianzhong1962@163.com) (J. Xu), [xcyang@tmmu.edu.cn](mailto:xcyang@tmmu.edu.cn) (X. Yang), [dongshiwu@tmmu.edu.cn](mailto:dongshiwu@tmmu.edu.cn) (S. Dong).

<https://doi.org/10.1016/j.bioactmat.2021.04.038>

Received 14 December 2020; Received in revised form 20 April 2021; Accepted 25 April 2021

2452-199X/© 2021 The Authors. Publishing services by Elsevier B.V. on behalf of KeAi Communications Co. Ltd. This is an open access article under the CC

BY-NC-ND license (<http://creativecommons.org/licenses/by-nc-nd/4.0/>).

barely resorb bone matrix and on the contrary, they are anabolic for angiogenesis via secreting platelet derived growth factor-BB (PDGF-BB) [16–18]. This unselective inhibition of BPs in pOCs and mOCs potentially explained why long-term antiresorptive therapy is not satisfying. We assumed that specific depletion of mOCs while preserving beneficial pOCs is a better anabolic strategy in treating osteoporosis. We previously designed and constructed a graphene oxide (GO) based miR-7b transfection system to block pOC fusion for pOC preservation [19]. However, the complexity of the construction and involvement of exogenous small RNA make the whole transfection system less applicable for clinical use. To realize this strategy simpler and more efficient, we harnessed the acid secretion differences between pOC and mOC to design bone-targeted pH-responsive nanomaterials.

Cerium nanoparticles have been reported with neuroprotective, radioprotective, anti-sepsis, anti-stroke and anti-tumor activities [20–24]. The surface  $Ce^{3+}:Ce^{4+}$  ratio governing the biological activity of cerium oxide nanoparticles can be influenced by different pH levels [25]. This property makes cerium oxide nanoparticles a pH-sensitive enzyme that can change its enzymatic activity from antioxidative to oxidative at a relative lower pH level [26]. In human body, the micro-environment of bone resorption lacuna acidified by mOCs (pH = 3–4) is ideal for triggering the oxidative enzyme activity of cerium oxide nanoparticles [27].

In this study, the CNS we designed exhibited oxidative activity in low-pH microenvironment created by mOC and increased reactive oxygen species (ROS) generation which in turn decreased the viability of mOCs. Meanwhile, the antioxidative CNS at neutral pH level has no effect in pOCs, which secured bone anabolism by generating PDGF-BB to increase mesenchymal stem cell (MSC) osteogenesis and endothelial progenitor cell (EPC) angiogenesis.  $\mu$ CT results suggest CNS was more effective in attenuating bone loss relative to the current first line bisphosphonate in treating ovariectomized (OVX) mice.

## 2. Methods and materials

### 2.1. Nanoparticles synthesis, modification and characterization

The cerium nanoparticles were prepared by microemulsion or thermal decomposition method as described previously [28]. For microemulsion method, Sodium bis-(2-ethylhexyl) sulfosuccinate (1.5 g) was dissolved in toluene (50 ml) and mixed with cerium nitrate solution (2.5 ml, 0.1 mol/l). The mixture was then stirred for 45 min at room temperature and adding of 5 ml H<sub>2</sub>O<sub>2</sub> (30%). The solution was stirred for 1 h and allowed to separate into two layers. The organic layers containing cerium nanoparticles were collected for surface modification. For thermal decomposition method, the cerium nitrate hexahydrate (0.434 g) was dissolved in oleylamine (0.802 g) and 1-octadecene (4 g). The mixture was stirred at 80 °C for 30 min and then heated to 260 °C for 2 h. After cooling to room temperature, 80 ml acetone was added and the nanoparticles were collected by centrifugation. Collected nanoparticles were washed for three times and dispersed in 10 ml hexane. For surface modification, alendronate was coated on cerium nanoparticles as anchor molecules for PEG-600. PEG diacid 600, N-(3-Dimethylaminopropyl)-N-ethylcarbodiimide (EDC) and N-Hydroxysuccinimide (NHS) were mixed in dichloromethane under magnetic stir for 8 h at room temperature. The solvent was removed by rotate evaporation. Alendronate and Na<sub>2</sub>CO<sub>3</sub> were dissolved in water added with prepared cerium nanoparticles and heated to 80 °C under magnetic stir for 12 h. After cooling to room temperature, the water layer containing nanoparticles was separated by centrifugation. Acetone was added to precipitate out the nanoparticles. Precipitated cerium nanoparticles were dialyzed in water with molecular weight cut off of 10 k for 24 h. The surface coating process for cerium nanoparticles synthesized by thermal decomposition method were similar to microemulsion method. Except that the nanoparticles were precipitate out from hexane by ethanol and redispersed in tetrahydrofuran, and the surface coating was carried out in

tetrahydrofuran/water system. For characterization of synthesized CNS, TEM analysis was conducted using a Tecnai G2 F20 S-TWIN TEM (200 kV). Samples were prepared by casting a drop of nanoparticle dispersion (water) onto a carbon-coated copper grid. NMR spectrum was measured using a DD2 600 MHz NMR spectrometer (Agilent). The nanoparticles were dried on EYELA FDU-2100 freeze drier for 48 h. TGA experiments were performed on TA Q50. Samples of the surface-modified nanoparticles were dried on EYELA FDU-2100 for 24 h before analysis. XPS measurements and spectrum intergration were performed using Scientific Escalab 250 (Thermo, UK). Photoelectron spectra was excited by Al K $\alpha$  (1486.6 eV) anodes at 100 W. The binding energy scale was calibrated from the C1s peak at 284.8 eV.

### 2.2. TEM analysis of CNS-cell interaction

BMMs were grown in chamber cell culture slides treated with or without RANKL (100 ng/ml) and M-CSF (50 ng/ml) with different concentrations of CNS for 72 h. The cells were fixed in 3% glutaraldehyde. Thin sections were then cut and placed on Formvar copper grids and then stained with uranyl acetate and lead citrate. After staining, the sections were examined on a FEI Tecnai 110 kV microscope at 80 kV, and digital photomicrographs were taken.

### 2.3. Average cellular pH level detection

Average cellular pH level detection was performed using LysoSensor Yellow/Blue dextran molecular probe (Life Technologies). In brief, BMMs (5 × 10<sup>3</sup> cells/well in 96-well plates) were cultured in  $\alpha$ -MEM medium (RANKL+, RANKL + CNS+) for 24 h, 72 h and 120 h and each well was replaced with  $\alpha$ -MEM medium. RANKL + represents RANKL (100 ng/ml) and M-CSF (50 ng/ml) and CNS + represents 100  $\mu$ g/ml. Intracellular pH level was measured by LysoSensor Yellow/Blue dextran, which indicates blue (Em 452 nm) at pH level of 4.0 and indicates green (Em 521 nm) at pH level of 7.0. Images were taken using the fluorescence microscopy (Olympus).

### 2.4. Oxidation kinetic analysis

The oxidase activity of CNS at pH 4.0 and 7.0 was tested using organic dye tetramethylbenzidine (TMB) as substrate according to previous method [14]. In detail, 10  $\mu$ g/ml CNS was mixed with 0.08 mM TMB in citrate buffer. Upon oxidation the TMB develop blue color which could be detected at 652 nm. The color change was recorded at interval of 30 s for 10 min using a Bio-TEK, Synergy H4 Microplate reader.

### 2.5. Statistical analysis

All data are representative of at least three experiments of similar results performed in triplicate unless otherwise indicated. Data are expressed as mean  $\pm$  SD. One-way ANOVA followed by Student-Newman-Keuls post hoc tests was used to determine the significance of difference between results, with \* $p$  < 0.05, \*\* $p$  < 0.01 being regarded as significant.

The complete detailed methods are provided in the online-only Data Supplement.

## 3. Results

### 3.1. Nanomaterial preparation, characterization, subcellular localization and toxicity

Cerium oxide nanoparticle used in our study were synthesized by microemulsion method as we previously reported [28]. In brief, after synthesis, alendronate was coated to the nanoparticles as an anchor. The surface of nanoparticles was then modified through an in situ ligand exchange method with PEG600 (Fig. 1a). Synthesized cerium

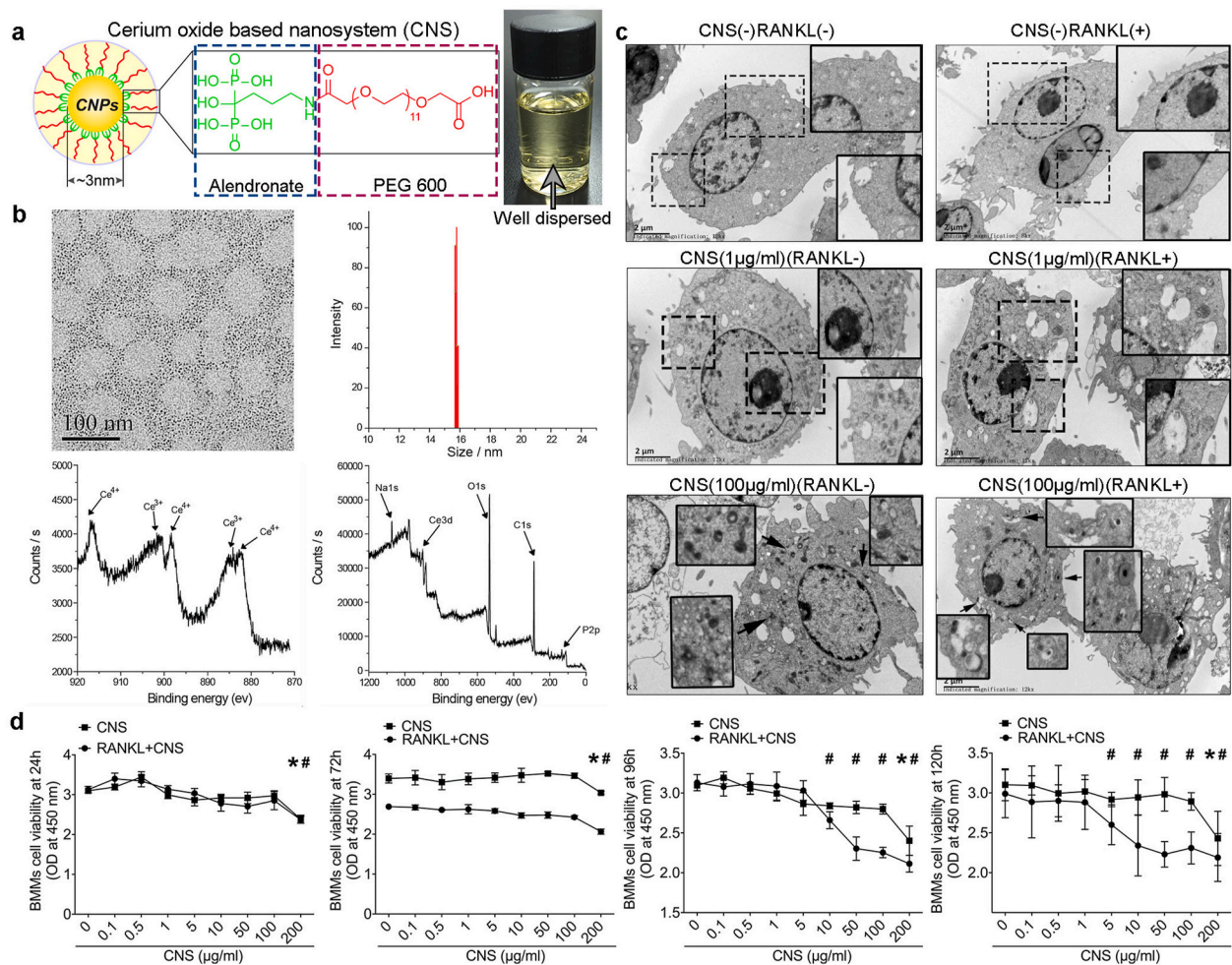


**Fig. 1. Nanoparticles preparation, characterization, subcellular localization and toxicity.** (a) Schematic illustration of CNS. Synthesized CNS was well dispersed in water with bright yellow color. (b) TEM image, hydrodynamic diameter and XPS spectra of CNS. (c) Subcellular localization of CNS in bone marrow macrophages (BMMs). (d) Cell viability evaluation of CNS in BMMs at 24 h, 72 h, 96 h and 120 h (\* among CNS groups, # among RANKL + CNS groups). The data in the figures represent the averages  $\pm$  SD. Significant differences are indicated as \*/# ( $p < 0.05$ ). (For interpretation of the references to color in this figure legend, the reader is referred to the Web version of this article.)

nano-system (CNS) showed increased stability and dispersion in water. The PEG ligand weight percentage of CNS was 51.7%, the hydrodynamic diameter was  $15.2 \pm 0.4$  nm and the  $\text{Ce}^{3+}$  concentration was 49.3% (Fig. 1b). CNS showed higher antioxidative activity and less cellular toxicity compared to naked cerium oxide nanoparticles [28]. Transmission Electron Microscope (TEM) analysis revealed that CNS was incorporated in membrane bound vesicles by bone marrow macrophages (BMMs) during receptor activator of nuclear factor  $\kappa$ B ligand (RANKL) induced osteoclastogenesis. CNS was found aggregated inside the cells as electron dense matters either free in cytoplasm or in vesicles (Fig. 1c). Cellular uptake of FITC conjugated CNS suggested no difference in pOC and mOC regardless of the dosages (Fig. S1). Cell viability test revealed that without RANKL treatment, CNS was not toxic until the dosage reached to 200  $\mu\text{g}/\text{ml}$ ; however, in the presence of RANKL, CNS showed an increased cytotoxicity and started to reduce cell viability when the dosage reached to 10  $\mu\text{g}/\text{ml}$  (96 h) and 5  $\mu\text{g}/\text{ml}$  (120 h) (Fig. 1d). Upon RANKL (100 ng/ml) stimulation, BMMs differentiate to mOCs at 96 h [29], immunoblots for cleaved caspase-3 in pOC and mOC at 0, 8 h, and 16 h after introduction of CNS (10  $\mu\text{g}/\text{ml}$ ) showed a remarkably increased in mOC, whereas pOC was barely affected (Fig. S2). To exclude the effects of RANK expression, we isolated primary mouse B cells,  $\text{CD4}^+$  T cells,  $\text{CD8}^+$  T cells, and neutrophils to evaluate the influence of CNS on the cell viability. The results showed that the CNS started to significantly decrease the cell viability of  $\text{CD4}^+$  T cells,

$\text{CD8}^+$  T cells, and neutrophils at the dosage of 200  $\mu\text{g}/\text{ml}$ , which is similar with BMMs. However, B cells seemed to be more susceptible to CNS treatment and the cell viability decreased from the dosage of 50  $\mu\text{g}/\text{ml}$  (Fig. S3). The above results suggested low dosage of CNS has specific cytotoxicity in mOCs.

### 3.2. CNS decreased the viability of mOCs *in vitro*

To understand the reason why CNS is specifically toxic in mOCs, we performed a time dependent cytoskeleton and focal adhesion stain assay (Fig. 2a), and found that in CNS-free group, OC number and average nuclei number increased over time and reached to its peak at 120h (Fig. 2b). However, BMMs treated with CNS bring forward the mOC formation peak from 120h to 96h (10  $\mu\text{g}/\text{ml}$ ) and 72h (100  $\mu\text{g}/\text{ml}$ ) respectively. Interestingly, in the presence of CNS, mOC failed to keep viable and vanished within the next 24 h. This result suggested CNS decreased the life span of mOCs. Accordingly, tartrate resistant acid phosphatase (TRAP) stain results showed that TRAP activity reached to the peak value at 120h upon RANKL stimulation; however, the peak time for CNS treated cells is 72h, followed by a decrease at 120h (Fig. 2c). Bone resorption assay results showed that the resorption pit areas in CNS treated groups were significantly higher compare with control groups at 72h. The two groups reached to similar resorption extent with no significant difference at 120h (Fig. 2d). Actin ring is a

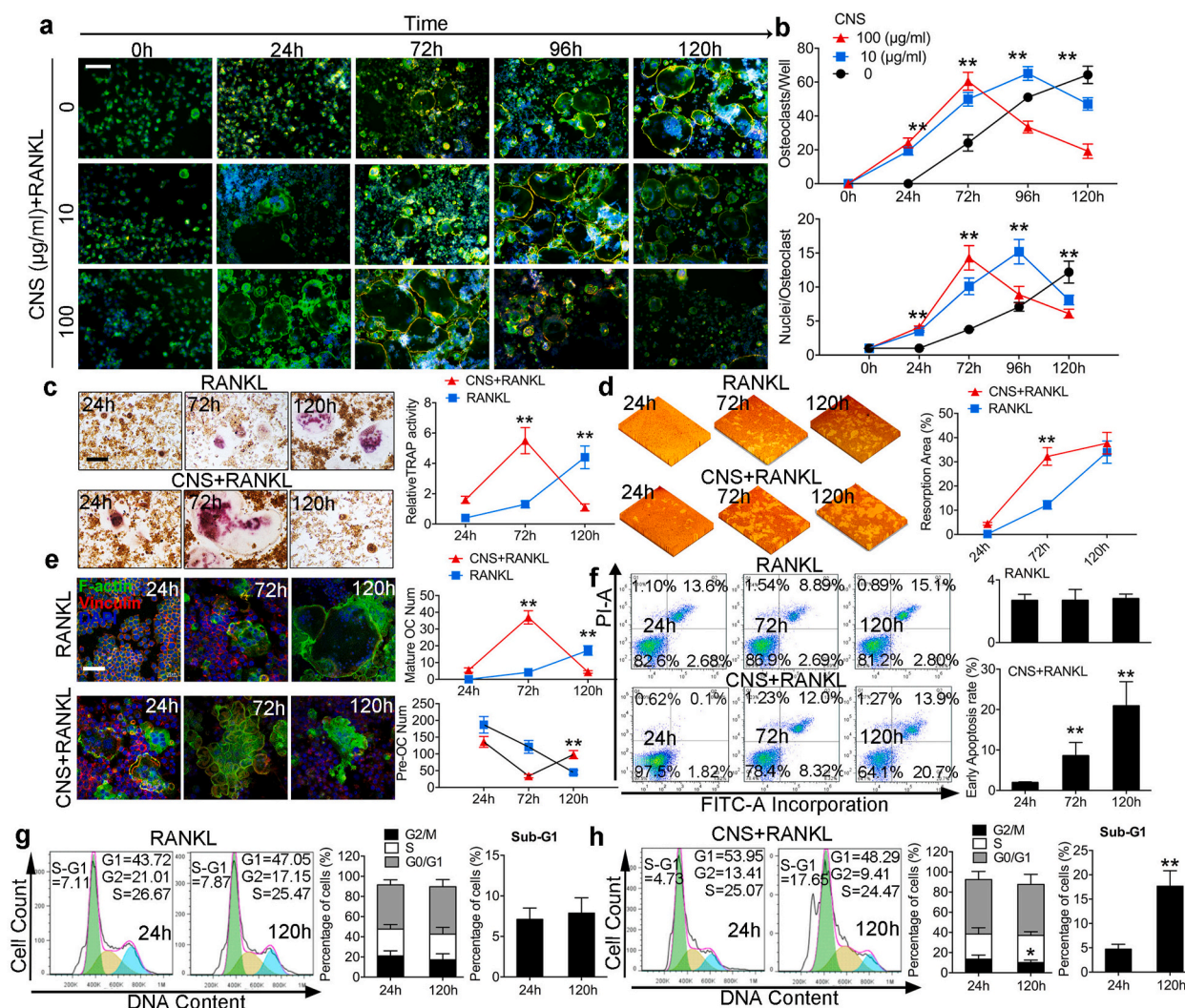


**Fig. 2.** CNS decreased the viability of mOCs *in vitro*. (a) Cytoskeleton and focal adhesion stain images of BMMs treated with CNS in a timeline, bar represents 200  $\mu\text{m}$ . (b) Quantification of OC number and OC average nuclei number. (c) TRAP stain images and quantification of relative TRAP activity, bar represents 200  $\mu\text{m}$ . (d) Pit formation assay images and quantification of resorption area. (e) Actin ring observation, quantification of mature OC number and POC number. (f) Annexin-V/PI staining analyzed by FCM quantifying early cell apoptotic rate. (g, h) Cell cycle and sub-G1 analysis of BMMs treated with RANKL alone (g) or together with CNS (h). Images are representative of  $n = 3$  independent experiments. The data in the figures represent the averages  $\pm$  SD. Significant differences are indicated as \*\* ( $p < 0.01$ ).

specified cellular structure of mOC, confocal microscopy results showed that the actin ring formation in CNS treated OCs robustly increased at 72h and significantly decreased at 120h; however, it is very excited to notice that mononuclear pOC number was not influenced by CNS (Fig. 2e). Flow cytometry (FCM) analysis showed that CNS significantly increased early cell apoptotic rate at 72h and 120h compare with the control groups (Fig. 2f). Meanwhile, G2/M cell proportion was decreased by CNS treatment suggesting a cell cycle arrest. The increased percentage of sub-G1 distribution by CNS treatment also suggested an increased cell apoptosis (Fig. 2g and h). FCM analysis was consistent with the staining results showing that OC was induced to apoptosis after its maturation. It is also worthy to mention that  $\text{Ce}^{3+}$  or CNS alone without RANKL cannot induce osteoclastogenesis (Fig. S4). Cell-cell fusion and osteoclast specific gene expression were also evaluated to confirm the promoting effects of CNS in RANKL induced osteoclastogenesis within 72h (Fig. S5). From the *in vitro* results, we concluded that CNS accelerated the process of RANKL induced osteoclastogenesis and then lead mOCs to apoptosis. Taken together, CNS decreased the viability of mOC.

### 3.3. CNS selectively increases ROS production and $\text{Ca}^{2+}$ oscillation in mOCs

*In vitro* results revealed that CNS has selective cytotoxicity in mOCs. To figure out the underlying mechanism, we then detected the micro-environment pH level change during osteoclastogenesis with or without CNS treatment (Fig. 3a). As shown in Fig. 3b, CNS treatment decreased the average pH level to 4.0 at 72h, the pH level was then restored to about 5.5 at 120h suggesting the decreasing number of mOCs. The low-pH microenvironment is acidified by mOCs through ATPase H + Transporting V0 Subunit D2 (ATP6v0d2), an essential proton pump responsible for extracellular acidification in bone resorption [30]. CNS treatment increased ATP6v0d2 expression in BMMs in a time-dependent way from 0h to 72h (Fig. 3c), which explained the decrease of pH level at 72h. In addition, oxidation kinetic studies revealed that the CNS acquired oxidative enzymatic activity immediately in the environment of pH level equals to 4.0. The oxidative enzymatic activity robustly increased for about 2 min and gradually stabilized after 3 min (Fig. 3d). These results suggest that the CNS interacting with mOCs are mostly oxidative. To find out the effects of oxidative CNS in mOCs, we

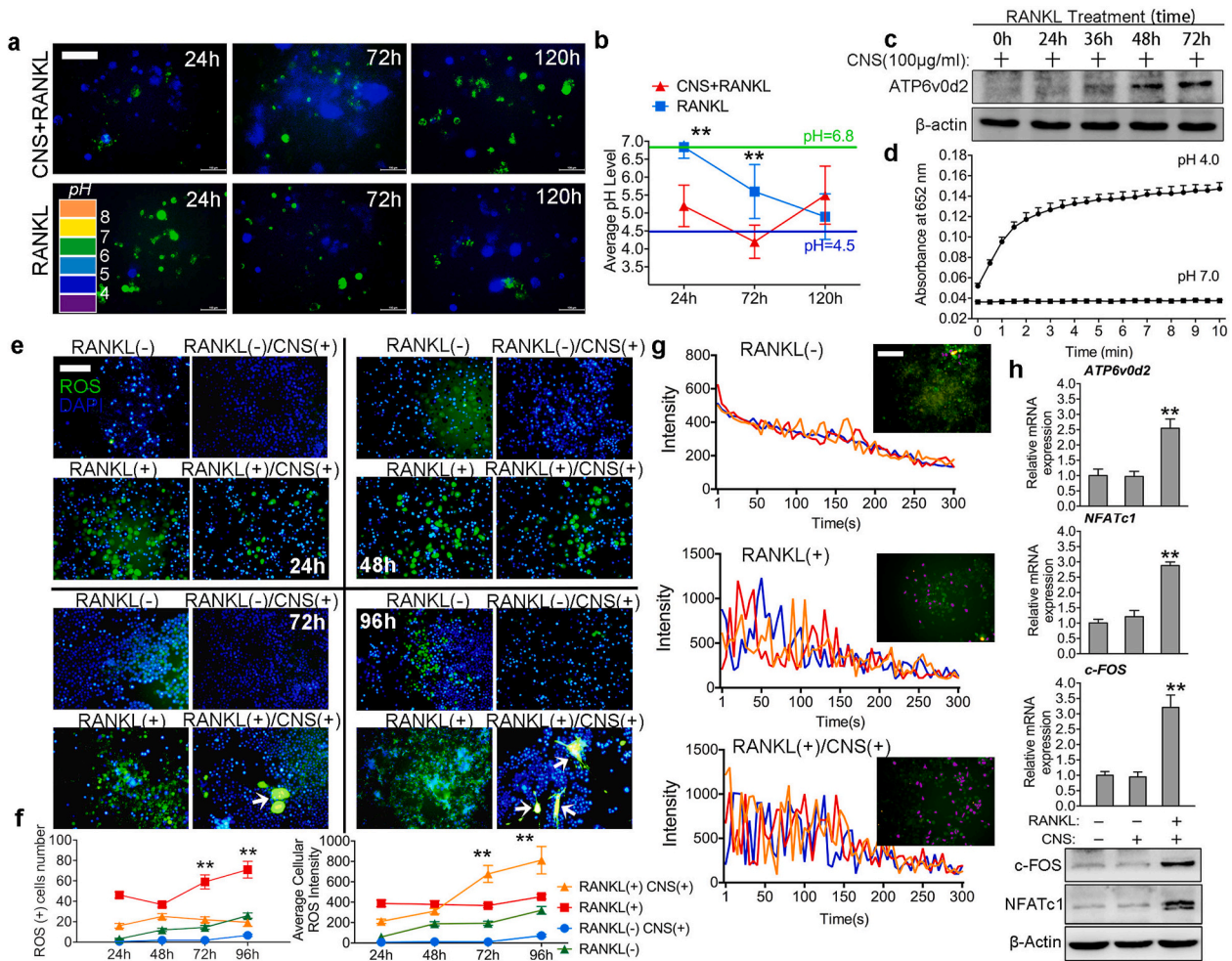


**Fig. 3.** CNS selectively increases ROS production and  $\text{Ca}^{2+}$  oscillation in mOCs. (a) Cellular pH detection during osteoclastogenesis, bar represents 200  $\mu\text{m}$ . (b) Quantification of average cellular pH level. (c) Western blot analysis of ATP6v0d2 expression. (d) Oxidation kinetic experiment testing oxidative enzymatic activity of CNS at pH 4.0 and pH 7.0. (e) Intracellular ROS detection of BMMs in a time line, bar represents 200  $\mu\text{m}$ . (f) Quantification of ROS positive cell number and average cellular ROS intensity. (g) Fluo-4 fluorescent images of BMMs at 72 h. Pseudo-color labeled (purple) area represents actively fluorescence ration changing cell, bar represents 400  $\mu\text{m}$ . Three representative traces are presented, fluorescence ratio change recorded every 5 s for 300 s. (h) Relative mRNA expression of *ATP6v0d2*, *NFATc1*, *c-FOS* and western blot images of *c-FOS*, *NFATc1* and  $\beta$ -actin. Images are representative of  $n = 3$  independent experiments. The data in the figures represent the averages  $\pm$  SD. Significant differences are indicated as \*\* ( $p < 0.01$ ). (For interpretation of the references to color in this figure legend, the reader is referred to the Web version of this article.)

performed reactive oxygen species (ROS) assay from 24h to 96h (Fig. 3e) and figured out that RANKL increased ROS(+) cell number with the increase of time but CNS had no influence on it. However, the average cellular ROS intensity was significantly increased (indicated by white arrows in Fig. 3e) by CNS treatment (Fig. 3f). This result means CNS did not increase the number of ROS(+) cells, instead, it only affected cells that were already accumulating ROS. This discovery confirmed our previous assumption that CNS only affects acid secreting mature OC through the oxidative activity acquired at a lower pH level. We also confirmed that CNS had no effect on pOCs because ROS(+) cell number was not increased. In bone remodeling, osteoclastic activity is associated with increased extracellular  $\text{Ca}^{2+}$  concentration and  $\text{Ca}^{2+}$  influx, which in turn affect RANKL-evoked  $\text{Ca}^{2+}$  signaling [4]. In our study, CNS enhanced both average amplitude and frequency of  $\text{Ca}^{2+}$  oscillation compare to BMMs treated with RANKL alone (Fig. 3g, Fig. S6). Intracellular ROS and  $\text{Ca}^{2+}$  signaling then activated downstream *c-Fos*/*NFATc1* (Fig. 3h) to enhance osteoclastogenesis. We also found that CNS treatment increased the mRNA expression of *CLCN7* but has no effect on *CA2* (Fig. S7). However, over generation of ROS finally lead to DNA damage causing cell cycle arrest and apoptosis in mOCs.

### 3.4. CNS attenuates bone loss in OVX mice

We then used OVX osteoporotic mouse model to test the *in vivo* effects of CNS. Mice were separated into four groups: sham group (sham operated), OVX group, low CNS dosage (10 mg/kg) group and high CNS dosage (100 mg/kg) group. CNS was dissolved in normal saline and injected intraperitoneally once a week for four weeks. Control groups received only normal saline. After euthanization, dissected femur trabecular and cortical bone was contoured for analysis using  $\mu\text{CT}$  (Fig. 4a). Quantification analysis showed that CNS administration (10 mg/kg and 100 mg/kg) in OVX mice significantly increased bone mineral density (BMD), trabecular bone volume fraction (BV/TV), trabecular number (Tb. N), trabecular thickness (Tb. Th), cortical bone thickness (Ct. Th), and decreased trabecular separation (Tb. Sp) ( $p < 0.01$ ) (Fig. 4b). We also tested the effects of CNS in normal wild type male mice at the age of 3 weeks and 8 weeks and found that CNS administration could also significantly increase bone volume and density in normal mice (Figs. S8 and S9). The *in vivo* results indicated that CNS administration attenuated bone loss in OVX mice.

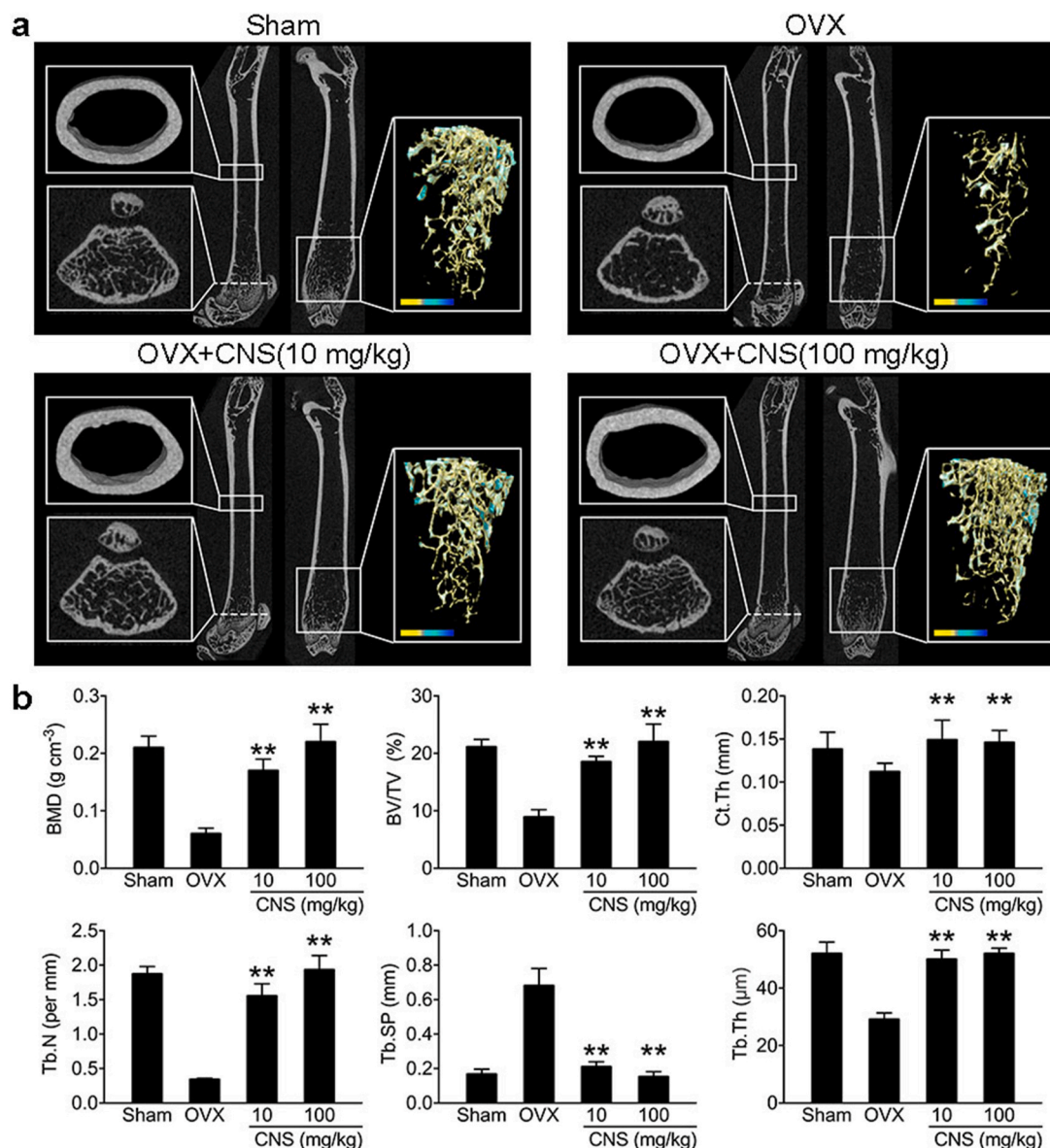


**Fig. 4.** CNS attenuates bone loss in OVX mice. (a) Representative  $\mu$ CT images of longitudinal section femurs, cross-sectional view of the distal femur and reconstructed trabecular structure of the ROI (white dashed box). Color scale bar represents bone mineral density level. Masson stain and TRAP stain images on the right. (b) Quantitative  $\mu$ CT analysis of bone mineral density (BMD), trabecular bone volume fraction (BV/TV), trabecular number (Tb. N), trabecular thickness (Tb. Th), cortical bone thickness (Ct. Th), and decreased trabecular separation (Tb. Sp). (c) Quantitative analysis of bone formation ratio and OC surface/bone surface ratio. Images are representative of  $n = 3$  independent experiments. The data in the figures represent the averages  $\pm$  SD. Significant differences are indicated as \*\* ( $p < 0.01$ ). (For interpretation of the references to color in this figure legend, the reader is referred to the Web version of this article.)

### 3.5. pOCs preserved by CNS induce osteogenesis and angiogenesis via FAK pathway

We then used BMMs and MSCs co-culture system (Fig. 5a) to compare CNS with a currently first-line antiresorptive drug alendronate (Ald). Because that Ald has no selectivity in depleting OCs, pOCs were also depleted and osteogenesis of MSCs was not detected (Fig. 5b). However, in CNS treated co-culture system, osteogenesis of MSCs was significantly induced characterized by increased ALP activity and Alp, Runx2 expression (Fig. 5b) suggesting that pOCs were preserved. In addition, we found both bone marrow PDGF-BB and VEGF concentrations were significantly increased in OVX mice administered with CNS compare to Ald, and no significance was detected in serum (Fig. 5c). Western blot results also confirmed that CNS increased PDGF-BB secretion while Ald had an inhibitory effect. We then co-cultured BMMs with the endothelia progenitor cells (EPCs) to observe tube

formation. CNS treatment significantly enhanced EPC tube formation compared with Ald (Fig. 5e). Focal adhesion kinase (FAK) is known to mediate MSC adhesion and EPC angiogenesis [31,32]. Western blot analysis showed that when co-cultured with BMMs, CNS induced phosphorylation of platelet-derived growth factor receptor  $\beta$  (PDGFR $\beta$ ) in both MSCs and EPCs by 5 min and peaked at 30 min (Fig. 5f). In addition, phosphorylation of downstream phosphatidylinositol 3-kinase (PI3K), Akt and FAK also peaked at 30 min (Fig. 5f). These results indicate PDGF-BB enhanced angiogenesis and osteogenesis through PI3K-Akt dependent activation of FAK.

### 3.6. CNS treatment protected bone loss in OVX mice better than alendronate via enhancing angiogenesis

Recent studies identified a special vessel subtype with distinct morphological, molecular properties and location, which is

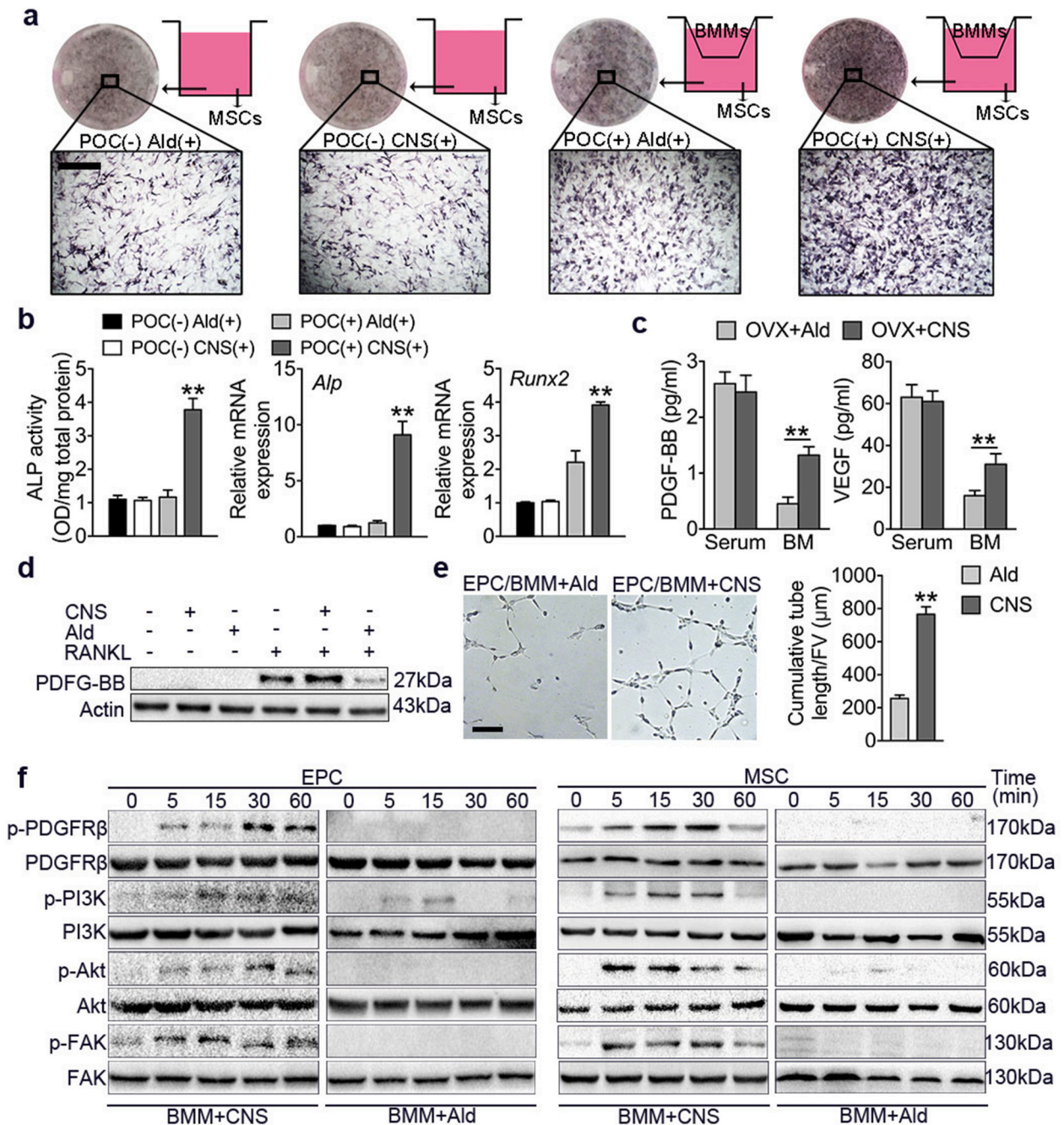


**Fig. 5. pOCs preserved by CNS induce osteogenesis and angiogenesis via FAK pathway.** (a) MSCs were cultured alone or co-cultured with BMMs in osteogenic media with Alendronate (Ald) or CNS treatment. ALP stain was performed on day 7. Bar represents 200 μm. (b) Quantification of ALP activity of MSCs. Relative mRNA expression levels of *Runx2* and *Alp*. (c) ELISA for serum or bone marrow (BM) PDGF-BB and VEGF concentrations. (d) Western blot analysis of PDGF-BB levels in BMMs in different culture conditions. (e) Matrigel tube formation assay images and quantitative analysis of cumulative tube length of EPC co-cultured with BMMs treated with Ald or CNS. Bar represents 150 μm. (f) Western blot analysis of the phosphorylation of PDGFRβ, PI3K, Akt and FAK in MSCs and EPCs co-cultured with BMMs treated with Ald or CNS for 5–60 min. Images are representative of n = 3 independent experiments. The data in the figures represent the averages ± SD. Significant differences are indicated as \*\* ( $p < 0.01$ ).

CD31<sup>hi</sup>Emcn<sup>hi</sup> vessel [33]. Their abundance is intimately associated with new bone formation. It has also been proved that PDGF-BB secreted by POCs induces the formation of CD31<sup>hi</sup>Emcn<sup>hi</sup> vessels in coupling bone formation [16]. We have already showed that pOCs preserved by CNS enhance angiogenesis *in vitro*. We then compared the *in vivo* effectiveness of CNS and Ald using OVX mice. CNS exhibited better results in restoring BMD and BV/TV compare to Ald, while trabecular indicators were not different (Fig. 6a). As expected, OVX mice had significantly higher number of osteoclast versus sham mice, while Ald

treated OVX mice barely had osteoclast. Of note, CNS treated OVX mice still have osteoclasts but were much more PDGF-BB positive (Fig. 6c and d). Consistently, CD31<sup>hi</sup>Emcn<sup>hi</sup> cell number was significantly higher in OVX mice treated with CNS compare to Ald (Fig. 6b). Moreover, CD31<sup>hi</sup>Emcn<sup>hi</sup> endothelial cell proportion in bone marrow was also the highest in CNS treated OVX mice (Fig. 6e). Microphil-perfused angiography demonstrated that vessel volume and surface were significantly increased in OVX mice treated with CNS than treated with Ald (Fig. 6f and g). The results suggest that CNS was more effective than Ald in

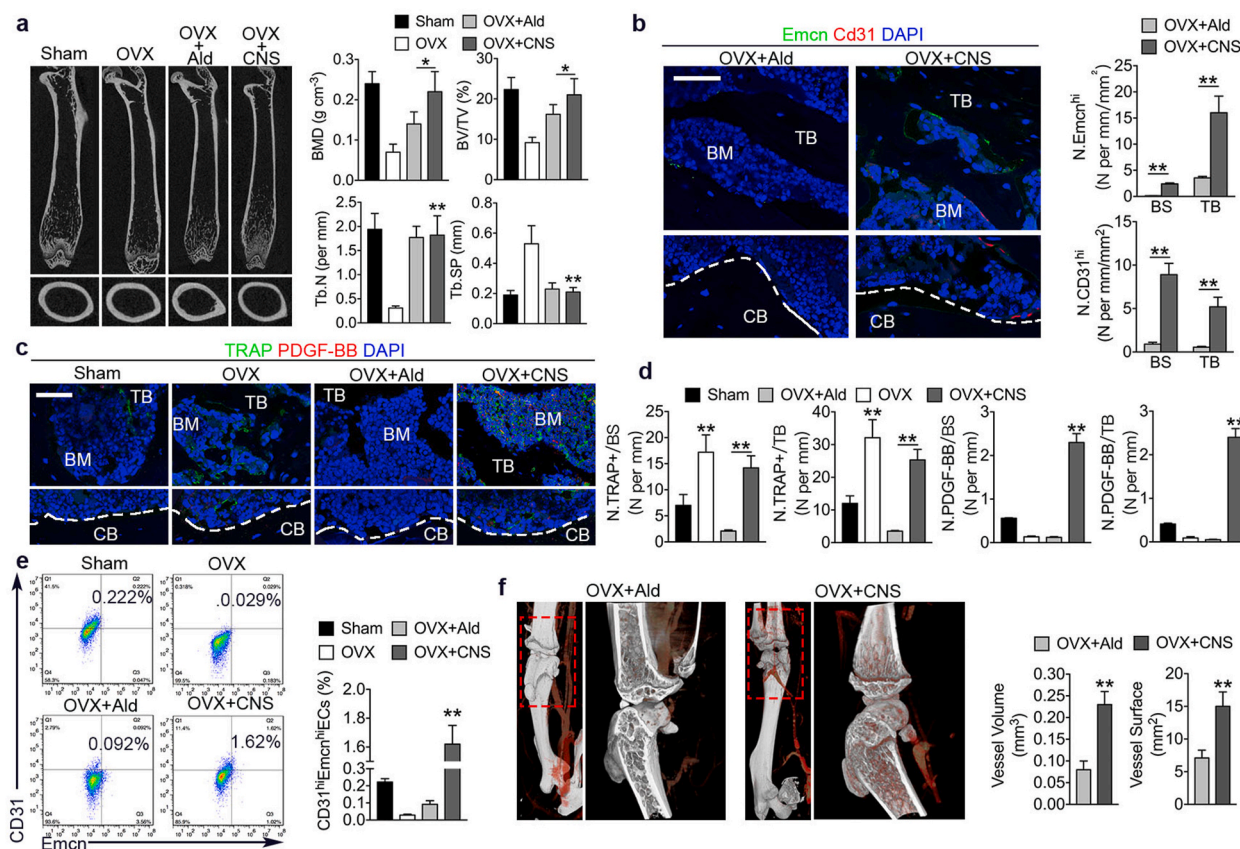


**Fig. 6.** CNS treatment protected bone loss in OVX mice better than alendronate via enhancing angiogenesis. (a) Representative  $\mu$ CT images of longitudinal section femurs, and quantification of bone mineral density (BMD), trabecular bone volume fraction (BV/TV), trabecular number (Tb. N), and decreased trabecular separation (Tb. Sp). (b) Immunostaining of CD31 (red) and Endomucin (green) with quantification of CD31<sup>hi</sup>Emcn<sup>hi</sup> cells in trabecular bone and bone surface (bottom). Bar represents 100  $\mu$ m. (c) Immunostaining of TRAP (green) and PDGF-BB (red) in trabecular bone and cortical bone. Bar represents 100  $\mu$ m. (d) Quantification of number of TRAP positive cells (N. TRAP+) and number of PDGF-BB positive cells (N.PDGF-BB) per respective bone surface (BS) or trabecular bone (TB). (e) Flow cytometry analysis (left) with quantification (right) of CD31<sup>hi</sup>Emcn<sup>hi</sup> cells in total bone marrow cells. (f)  $\mu$ CT microphil-perfused angiography of OVX mice femurs treated with Ald or CNS and quantification of vessel volume and surface. Images are representative of  $n = 5$  independent experiments. The data in the figures represent the averages  $\pm$  SD. Significant differences are indicated as \* ( $p < 0.05$ ) or \*\* ( $p < 0.01$ ). (For interpretation of the references to color in this figure legend, the reader is referred to the Web version of this article.)

treating OVX osteoporotic mice via enhancing angiogenesis through preserving pOCs.

### 3.7. CNS treatment in OVX mice showed overall anabolic effects

To examine the overall effects of CNS treatment in OVX mice, we further evaluated the bone formation using double labeling by injecting OVX mice with Calcein and Alizarin red (Fig. 7a). The results showed that both bone formation rate (BFR)/bone surface (BS), mineral apposition rate (MAR) and mineralizing surface (MS)/BS were significantly higher in OVX mice treated with CNS regardless of the dosages (10 mg/kg or 100 mg/kg) (Fig. 7b). We then tested the change of bone turnover markers and found that the decrease of bone formation marker P1NP in OVX mice was rescued by CNS treatment as expected. The increase of CTX in OVX mice was also partially brought down by CNS treatment (Fig. 7c). To test the bone strength, femurs from OVX mice with different treatments were subjected to a three-point bending mechanical testing. The results showed that the ultimate load and stiffness were both decreased in OVX mice, CNS treatment of 10 mg/kg partially rescued the decrease, CNS of 100 mg/kg even increased the bone strength relative to the sham groups (Fig. 7d). These results suggest that CNS treatment in OVX osteoporotic mice showed overall anabolic effects.

## 4. Discussion

It is worthy to notice that Ca<sup>2+</sup> and ROS have mutual reinforcing effects. ROS can sensitize endoplasmic reticulum (ER)-based calcium channels leading to the release of calcium from the ER into the cytosol to concentrate in the inner matrix of mitochondria, where it disrupts the electron-transport chain leading to the production of more ROS. These mitochondria produced ROS can further exacerbate calcium release from the ER, resulting in the accumulation of ROS to a toxic level [34]. It is also reported that cerium nanoparticle is toxic to human peripheral blood monocytes via mitochondrial apoptosis [17]. Sub-cellular distribution of cerium nanoparticle uptake revealed its co-localization with mitochondria, lysosomes and ER [35]. These findings reinforced our results that osteoclastogenesis was accelerated in the first place but quickly ended up with apoptosis afterwards. In total, the viability of mature osteoclasts was decreased.

pH-sensitive nano-systems have been developed targeting the acidic environment of tumor [36,37]. Studies have already shown that pH-sensitive drug delivery systems could improve cancer treatment efficiency [38]. Apart from tumor microenvironment, the physiological pH change in the gastrointestinal tract was also utilized to develop pH-responsive drug delivery systems [39]. During bone remodeling, the pH level of resorption lacuna reaches to 3–4. The low-pH microenvironment is acidified by OCs through ATP6v0d2 for inorganic bone matrix degradation and activation of pH-sensitive enzymes [30].

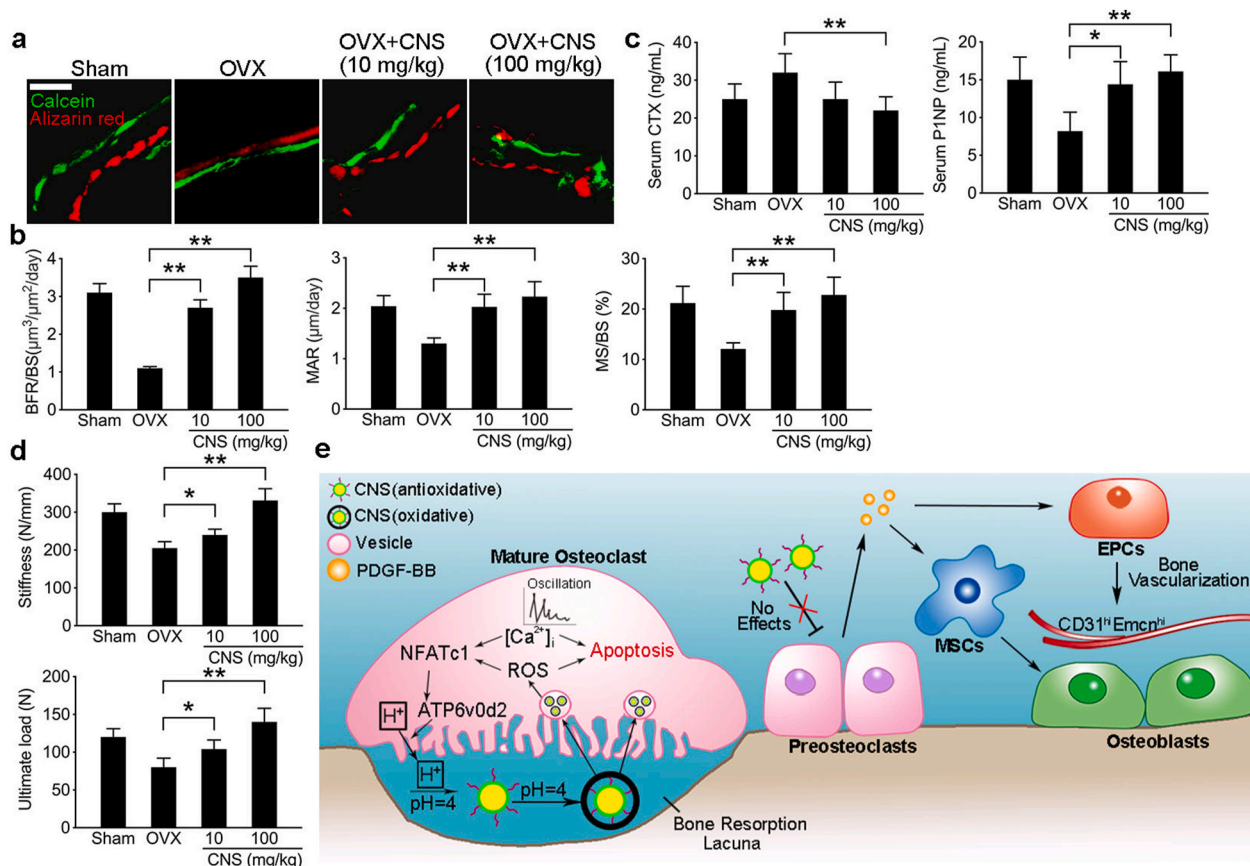


**Fig. 7. CNS treatment in OVX mice showed overall anabolic effects.** (a) Representative images of histologic sections showing calcein and alizarin red double-labeling of endocortical bone in femur mid diaphysis of CNS treated OVX mice and their control mice. bar represents 200  $\mu\text{m}$ . (b) Quantification of BFR (bone formation rate)/BS (bone surface), MAR (mineral apposition rate) and MS (mineralizing surface)/BS (bone surface). (c) Quantification of mouse serum CTX and P1NP in indicated groups. (d) 3-point bending tests of collected mouse femur in indicated groups with quantification of stiffness and ultimate load. (e) Schematic diagram of the mechanism of CNS functioning as a pro-anabolic therapy in treating OVX mice. Images are representative of  $n = 5$  independent experiments. The data in the figures represent the averages  $\pm$  SD. Significant differences are indicated as \* ( $p < 0.05$ ) or \*\* ( $p < 0.01$ ). (For interpretation of the references to color in this figure legend, the reader is referred to the Web version of this article.)

Meanwhile, ATP6v0d2 is also a necessary regulator for cell-cell fusion during osteoclastogenesis [40,41]. Dysregulation of osteoclasts can lead to various bone disorders including osteoporosis, rheumatoid arthritis and osteoarthritis or even aggravate bone metastases [42]. But do we treat the osteoclasts in these disorders universally without further sub-grouping? From monocyte/macrophage to mononuclear POC and then multinucleated polarized giant mature OC, although the stimulator RANKL and master regulator NFATc1 remain unchanged, OC at different stages varies greatly in both functioning and coupling with other cells. However, current OC targeting therapy hardly makes any differences among OCs at different stages [1]. We managed to selectively deplete mOCs while pOCs and their function were preserved. This made CNS has better efficacy in treating osteoporotic OVX mice compared with the current first-line antiresorptive drug Ald.

## 5. Conclusions

In our study, we used bone favored pH-responsive CNS to target the acidic microenvironment created by mOCs. Antioxidative CNS converted to oxidative further increased ROS accumulation and calcium oscillation, which significantly decreased the viability of mature OC. However, unconverted CNS had no effect on non-acid secreting pOCs. Therefore, anabolic effect of pOCs was preserved and PDGF-BB secretion enhanced MSCs migration, osteogenesis and EPCs angiogenesis (Fig. 7e). Animal study showed that CNS is more effective in attenuating bone loss in osteoporotic OVX mice compared with Ald. Our findings

provided an mOC-targeted drug delivery strategy with anabolic effects in treating bone disorders with excessive bone loss.

## Data and materials availability

All data generated or analyzed during this study are included in this article (and its supplementary information files). Please contact the corresponding author for unique material requests. Some material used in the reported research may require requests to collaborators and agreements with both commercial and non-profit institutions, as specified in the paper. Requests are reviewed by Army Medical University to verify whether the request is subject to any intellectual property or confidentiality obligations. Any material that can be shared will be released via a Material Transfer Agreement.

## CRediT authorship contribution statement

**Ce Dou:** conducted most of the experiments and prepared the manuscript, conceived the idea, supervised. the project. helped in planning the projects and provided suggestions for experiments, wrote the manuscript. **Jianmei Li:** started the project and did some of the experiments. **Jian He:** started the project and did some of the experiments. **Fei Luo:** helped with some of for the experiments. **Tao Yu:** helped with some of for the experiments. **Qijie Dai:** helped in planning the projects and provided suggestions for experiments. **Yueqi Chen:** helped in planning the projects and provided suggestions for

experiments. **Xiaochao Yang**: helped in planning the projects and provided suggestions for experiments. **Shiwu Dong**: conceived the idea, supervised the project, helped in planning the projects and provided suggestions for experiments, wrote the manuscript.

#### Declaration of competing interest

No conflict of interest exists in the submission of this manuscript, and manuscript is approved by all authors for publication. I would like to declare on behalf of my co-authors that the work described was original research that has not been published previously, and not under consideration for publication elsewhere, in whole or in part. All the authors listed have approved the manuscript that is enclosed. I hope this paper is suitable for *Bioactive Materials*.

#### Acknowledgements

This work was funded by the State Key Program of National Natural Science of China (No. 81930067), the Nature Science Foundation of China (81802166), and AMU Southwest Hospital funding for young investigators (XZ-2019-505-005).

#### Appendix A. Supplementary data

Supplementary data to this article can be found online at <https://doi.org/10.1016/j.bioactmat.2021.04.038>.

#### References

- [1] W.J. Boyle, W.S. Simonet, D.L. Lacey, Osteoclast differentiation and activation, *Nature* 423 (2003) 337–342. DOI|.
- [2] H. Yasuda, et al., Osteoclast differentiation factor is a ligand for osteoprotegerin/osteoclastogenesis-inhibitory factor and is identical to TRANCE/RANKL, *Proc. Natl. Acad. Sci. U. S. A.* 95 (1998) 3597–3602. DOI|.
- [3] D.L. Lacey, et al., Osteoprotegerin ligand is a cytokine that regulates osteoclast differentiation and activation, *Cell* 93 (1998) 165–176. DOI|.
- [4] S.Y. Hwang, J.W. Putney Jr., Calcium signaling in osteoclasts, *Biochim. Biophys. Acta* 1813 (2011) 979–983. DOI|.
- [5] P. Li, et al., Fluid flow-induced calcium response in osteoclasts: signaling pathways, *Ann. Biomed. Eng.* 42 (2014) 1250–1260. DOI|.
- [6] G.D. Roodman, Advances in bone biology: the osteoclast, *Endocr. Rev.* 17 (1996) 308–332. DOI|.
- [7] S.L. Teitelbaum, Bone resorption by osteoclasts, *Science* 289 (2000) 1504–1508. DOI|.
- [8] S.C. Manolagas, Birth and death of bone cells: basic regulatory mechanisms and implications for the pathogenesis and treatment of osteoporosis, *Endocr. Rev.* 21 (2000) 115, 37 DOI|.
- [9] T.D. Rachner, S. Khosla, L.C. Hofbauer, Osteoporosis: now and the future, *Lancet* 377 (2011) 1276–1287. DOI|.
- [10] C. Sobacchi, et al., Osteopetrosis: genetics, treatment and new insights into osteoclast function, *Nat. Rev. Endocrinol.* 9 (2013) 522, 36 DOI|.
- [11] B. Le Goff, et al., Osteoclasts in RA: diverse origins and functions, *Joint Bone Spine* 80 (2013) 586–591. DOI|.
- [12] S.R. Cummings, L.J. Melton, Epidemiology and outcomes of osteoporotic fractures, *Lancet* 359 (2002) 1761, 7 DOI|.
- [13] J.Y. Reginster, N. Burlet, Osteoporosis: a still increasing prevalence, *Bone* 38 (2006) S4, 9 DOI|.
- [14] R.A. Adler, et al., Managing osteoporosis in patients on long-term bisphosphonate treatment: report of a task force of the American society for bone and mineral research, *J. Bone Miner. Res.* 31 (2016) 1910 (DOI|).
- [15] N. Ding, et al., Alendronate induces osteoclast precursor apoptosis via peroxisomal dysfunction mediated ER stress, *J. Cell. Physiol.* 233 (2018) 7415–7423. DOI|.
- [16] H. Xie, et al., PDGF-BB secreted by preosteoclasts induces angiogenesis during coupling with osteogenesis, *Nat. Med.* 20 (2014) 1270, 8 DOI|.
- [17] A. Teti, Mechanisms of osteoclast-dependent bone formation, *BoneKey Rep.* 2 (2013) 449. DOI|.
- [18] A.P. Kusumbe, R.H. Adams, Osteoclast progenitors promote bone vascularization and osteogenesis, *Nat. Med.* 20 (2014) 1238, 40 DOI|.
- [19] C. Dou, et al., Graphene-based MicroRNA transfection blocks preosteoclast fusion to increase bone formation and vascularization, *Adv. Sci.* 5 (2018) 1700578. DOI|.
- [20] J. Chen, et al., Rare earth nanoparticles prevent retinal degeneration induced by intracellular peroxides, *Nat. Nanotechnol.* 1 (2006) 142, 50 DOI|.
- [21] J. Colon, et al., Cerium oxide nanoparticles protect gastrointestinal epithelium from radiation-induced damage by reduction of reactive oxygen species and upregulation of superoxide dismutase 2, *Nanomedicine* 6 (2010) 698–705 (DOI|).
- [22] V. Selvaraj, et al., Effect of cerium oxide nanoparticles on sepsis induced mortality and NF-kappaB signaling in cultured macrophages, *Nanomedicine (Lond)* 10 (2015) 1275, 88 DOI|.
- [23] F. Biba, et al., A novel cytotoxic cerium complex: aquatrithloridobis(1,10-phenanthroline)cerium(III) (KP776). Synthesis, characterization, behavior in H<sub>2</sub>O, binding towards biomolecules, and antiproliferative activity, *Chem. Biodivers.* 6 (2009) 2153, 65 DOI|.
- [24] C.K. Kim, et al., Ceria nanoparticles that can protect against ischemic stroke, *Angew Chem. Int. Ed. Engl.* 51 (2012) 11039–11043. DOI|.
- [25] J.M. Dowding, et al., Cellular interaction and toxicity depend on physicochemical properties and surface modification of redox-active nanomaterials, *ACS Nano* 7 (2013) 4855, 68 DOI|.
- [26] A. Asati, et al., Oxidase-like activity of polymer-coated cerium oxide nanoparticles, *Angew Chem. Int. Ed. Engl.* 48 (2009) 2308, 12 DOI|.
- [27] A. Cappariello, et al., The great beauty of the osteoclast, *Arch. Biochem. Biophys.* 558 (2014) 70, 8 DOI|.
- [28] J. Xiang, et al., Cerium oxide nanoparticle modified scaffold interface enhances vascularization of bone grafts by activating calcium channel of mesenchymal stem cells, *ACS Appl. Mater. Interfaces* 8 (2016) 4489, 99 DOI|.
- [29] C. Dou, et al., Changing expression profiles of lncRNAs, mRNAs, circRNAs and miRNAs during osteoclastogenesis, *Sci. Rep.* 6 (2016) 21499. DOI|.
- [30] H. Wu, G. Xu, Y.P. Li, Atp6v0d2 is an essential component of the osteoclast-specific proton pump that mediates extracellular acidification in bone resorption, *J. Bone Miner. Res.* 24 (2009) 871, 85 DOI|.
- [31] H. Lv, et al., Mechanism of regulation of stem cell differentiation by matrix stiffness, *Stem Cell Res. Ther.* 6 (2015) 103. DOI|.
- [32] X. Zhao, J.L. Guan, Focal adhesion kinase and its signaling pathways in cell migration and angiogenesis, *Adv. Drug Deliv. Rev.* 63 (2011) 610, 5 DOI|.
- [33] A.P. Kusumbe, S.K. Ramasamy, R.H. Adams, Coupling of angiogenesis and osteogenesis by a specific vessel subtype in bone, *Nature* 507 (2014) 323–328. DOI|.
- [34] K. Zhang, R.J. Kaufman, From endoplasmic-reticulum stress to the inflammatory response, *Nature* 454 (2008) 455, 62 DOI|.
- [35] S. Singh, et al., Unveiling the mechanism of uptake and sub-cellular distribution of cerium oxide nanoparticles, *Mol. Biosyst.* 6 (2010) 1813, 20 DOI|.
- [36] E.S. Lee, K. Na, Y.H. Bae, Super pH-sensitive multifunctional polymeric micelle, *Nano Lett.* 5 (2005) 325, 9 DOI|.
- [37] J.K. Kim, et al., Novel pH-sensitive polyacetal-based block copolymers for controlled drug delivery, *Int. J. Pharm.* 401 (2010) 79–86 (DOI|).
- [38] M. Shen, et al., Multifunctional drug delivery system for targeting tumor and its acidic microenvironment, *J. Contr. Release* 161 (2012) 884, 92 DOI|.
- [39] H. Du, et al., The design of pH-sensitive chitosan-based formulations for gastrointestinal delivery, *Drug Discov. Today* 20 (2015) 1004, 11 DOI|.
- [40] S.H. Lee, et al., v-ATPase V0 subunit d2-deficient mice exhibit impaired osteoclast fusion and increased bone formation, *Nat. Med.* 12 (2006) 1403, 9 DOI|.
- [41] K. Kim, et al., NFATc1 induces osteoclast fusion via up-regulation of Atp6v0d2 and the dendritic cell-specific transmembrane protein (DC-STAMP), *Mol. Endocrinol.* 22 (2008) 176, 85 DOI|.
- [42] G. Russell, et al., Clinical disorders of bone resorption, *Novartis Found. Symp.* 232 (2001) 251–267, discussion 267–71 DOI|.